Computational study of forced air-convection in open-cathode polymer electrolyte fuel cell stacks

A.P. Sasmito[a], K.W. Lum[b], E. Birgersson[c,*], A.S. Mujumdar[a]

[a] *Department of Mechanical Engineering, National University of Singapore, 9 Engineering Drive 1, Singapore 117575, Singapore*
[b] *Institute of High Performance Computing, Fusionopolis Way, #16-16 Connexis, Singapore 138632, Singapore*
[c] *Department of Chemical and Biomolecular Engineering, National University of Singapore, 5 Engineering Drive 2, Singapore 117576, Singapore*

ARTICLE INFO

ABSTRACT

A mathematical model for a polymer electrolyte fuel cell (PEFC) stack with an open-cathode manifold, where a fan provides the oxidant as well as cooling, is derived and studied. In short, the model considers two-phase flow and conservation of mass, momentum, species and energy in the ambient and PEFC stack, as well as conservation of charge and a phenomenological membrane and agglomerate model for the PEFC stack. The fan is resolved as an interfacial condition with a polynomial expression for the static pressure increase over the fan as a function of the fan velocity. The results suggest that there is strong correlation between fan power rating, the height of cathode flow-field and stack performance. Further, the placement of the fan – either in blowing or suction mode – does not give rise to a discernable difference in stack performance for the flow-field considered (metal mesh). Finally, it is noted that the model can be extended to incorporate other types of flow-fields and, most importantly, be employed for design and optimization of forced air-convection open-cathode PEFC stacks and adjacent fans.

© 2010 Elsevier B.V. All rights reserved.

1. Introduction

The operation of a polymer electrolyte fuel cell (PEFC) stack with an open-cathode manifold involves transport of both air to and from the ambient and fuel from storage or a reformer. The magnitude of the inlet flow and the type of device – fan, pump, compressor, and/or blower – that is employed to provide the flow depends on the size, power and operating conditions of the fuel cell stack. Broadly speaking, the flow rates for the anode and cathode require careful consideration of the flow rate: (i) a high flow rate provides a high stoichiometric oxidant or fuel supply, but may cause dehydration of the membrane, where the former is beneficial and the latter is detrimental to stack performance; (ii) a low flow rate may give rise to flooding or depletion of oxygen or fuel, resulting in a drop in stack performance. In addition, the flow rate has to be sufficiently large to prevent overheating of the stack if it is also to be used for cooling purposes.

Depending on the size of the PEFC stack, the air flow for the cathodes can be provided by either natural convection due to temperature and concentration differences between the stack and the ambient (PEFC stacks with a power rating $\lesssim 100\,W$ [1]) or by forced convection (stacks with a power rating of around 100–1000 W

[1,2]). If fans are chosen to provide the airflow, it is important to ensure that they not only provide an adequate air flow rate through the cathodes in the stack, but also require minimal power in order to reduce the parasitic load, a compatible voltage rating with the stack and, to a lesser extent, a high life expectancy and generate a minimum of audible noise. A typical PEFC stack with an open-cathode manifold and a fan is illustrated in Fig. 1, where the fan is placed at the front of the stack (blowing mode) as opposed to the exit of the stack (suction mode).

To date, various designs and operating conditions of PEFC stacks equipped with free-breathing or forced-convection open-cathode manifolds have been studied experimentally (see, for example [3–11]). While these experimental studies provide details and insight into overall stack behaviour, they cannot do so at a local level; that is to say, at any given point inside the stack. Mathematical modeling and numerical simulations, on the other hand, can resolve not only global behaviour, for example, in terms of polarization curves, but also local behaviour, provided the essential phenomena have been adequately captured in the model. Several computational studies have been carried out for PEFC stacks [12–16] and for single cells with the ambient included [17–23]. The latter studies focus on free-breathing PEFCs, where the supply of oxygen from the air and removal of water from the stack occurs by natural convection; none of these studies have considered an open-cathode manifold with one or several fans providing forced convection through the stack, where the fan is included in the model itself.

Nomenclature

a	water activity
$a^{(l)}$	surface area of the agglomerates including water per unit volume, m^{-1}
$a^{(p)}$	surface area of the agglomerates per unit volume of catalyst layer, m^{-1}
A_{cl}	catalyst area, m^2
A_{fan}	total area of the fan, m^2
$c_i^{(g)}$	molar concentration of species i, $mol\,m^{-3}$
$c_{i,ref}^{(g)}$	reference molar concentration of species i, $mol\,m^{-3}$
$c_p^{(g)}$	specific heat capacity of gas mixture, $J\,kg^{-1}\,K^{-1}$
$c_{p,i}^{(g)}$	specific heat capacity of species i, $J\,kg^{-1}\,K^{-1}$
c_r	condensation/evaporation rate constant, s^{-1}
$\mathfrak{C}_1, \mathfrak{C}_2, \mathfrak{C}_3, \mathfrak{C}_4, \mathfrak{C}_5, \mathfrak{C}_6, \mathfrak{C}_7, \mathfrak{C}_8$	constants for the fan characteristic curve; $Pa\,s^7\,m^{-7}$, $Pa\,s^6\,m^{-6}$, $Pa\,s^5\,m^{-5}$, $Pa\,s^4\,m^{-4}$, $Pa\,s^3\,m^{-3}$, $Pa\,s^2\,m^{-2}$, $Pa\,s\,m^{-1}$, Pa
$\mathfrak{c}_1, \mathfrak{c}_2, \mathfrak{c}_3, \mathfrak{c}_4$	constants for the saturation pressure of water; –, K^{-1}, K^{-2}, K^{-3}
$D^{(c)}$	capillary diffusion, $m^2\,s^{-1}$
$D_i^{(g)}, D_{i,eff}^{(g)}$	diffusivity and effective diffusivity of species i, $m^2\,s^{-1}$
$D_{H_2O}^{(m)}$	diffusivity of water in the membrane, $m^2\,s^{-1}$
$D_{O_2,eff}^{(agg)}$	effective diffusion coefficient of oxygen in the ionomer inside the agglomerate, $m^2\,s^{-1}$
$D_{O_2}^{(l)}, D_{O_2}^{(p)}$	diffusion coefficient of oxygen in liquid water and in polymer film, $m^2\,s^{-1}$
$\mathbf{e}_y$	coordinate vector in y direction
E_a	activation energy, $J\,mol^{-1}$
E_{cell}	cell voltage, V
E_{rev}	reversible cell potential, V
E_{stack}	stack voltage, V
F	Faraday's constant, $A\,s\,mol^{-1}$
h_j	height of layer j, m
$H_{O_2}^{(l)}, H_{O_2}^{(p)}$	Henry's constant for air–water and air-polymer interfaces, $Pa\,m^3\,mol^{-1}$
H_{vap}	heat of vaporization, $J\,kg^{-1}$
$\mathfrak{H}$	relative humidity, %
$i, \mathbf{i}$	current density, $A\,m^{-2}$
$j_{a,c}^{ref}$	anode and cathode volumetric reference exchange current density, $A\,m^{-3}$
J	volumetric current density, $A\,m^{-3}$
$\mathcal{J}$	Leverett function
k	thermal conductivity, $W\,m^{-1}\,K^{-1}$
k_c	reaction rate constant, s^{-1}
L	length of the channel, m
$\mathfrak{k}_1$	constant, $V\,K^{-1}$
$\mathfrak{L}^{(C)}, \mathfrak{L}^{(p)}, \mathfrak{L}^{(Pt)}$	carbon, polymer, and platinum loading, $kg\,m^{-2}$
$\dot{m}_{H_2O}$	interphase mass transfer due to condensation or evaporation of water, $kg\,m^{-3}\,s^{-1}$
$M^{(g)}$	mean molecular mass of the gas phase, $kg\,mol^{-1}$
M_i	molecular mass of species i, $kg\,mol^{-1}$
$M^{(m)}$	equivalent weight of the dry membrane, $kg\,mol^{-1}$
$n^{(agg)}$	number of agglomerates per unit volume, m^{-3}
n_{cell}	number of cells in the stack
n_d	electroosmotic drag coefficient
$\mathbf{n}_i^{(g)}$	mass flux of species i, $kg\,m^{-2}\,s^{-1}$
$p^{(c)}$	capillary pressure, Pa
$p^{(g)}$	gas pressure, Pa
$p_{H_2O}^{sat}$	saturation pressure of water, Pa

P	power, W
R	gas constant, $J\,mol^{-1}\,K^{-1}$
$r^{(agg)}$	radius of agglomerate, m
s	liquid saturation
S	source term
$\mathfrak{T}_0, \mathfrak{T}_1, \mathfrak{T}_2$	constants, K
T	temperature, K
$\mathbf{u}, u, v, U$	velocities, $m\,s^{-1}$
V	volume, m^3
$x_i^{(g)}$	molar fraction of species i
x, y, z	coordinates, m
$\omega_i^{(g)}$	mass fraction of species i
$\omega^{(p)}$	mass fraction of polymer loading
$\omega^{(Pt)}$	mass fraction of platinum loading on carbon

Greek

α	transfer coefficient
$\beta^{(m)}$	modification factor
γ	volume fraction
δ	thickness of the film, m
Δ	difference
ε	porosity
η	overpotential, V
θ	wetting angle
κ	permeability, m^2
λ	water content
μ	dynamic viscosity, $kg\,m^{-1}\,s^{-1}$
ξ_1, ξ_2, ξ_3	correction factors for the agglomerate model
ρ	density, $kg\,m^{-3}$
τ	surface tension, $N\,m^{-2}$
$\boldsymbol{\sigma}$	total stress tensor, $N\,m^{-2}$
$\sigma^{(m)}$	protonic conductivity, $S\,m^{-1}$
$\sigma^{(s)}$	electric conductivity, $S\,m^{-1}$
$\phi^{(m)}$	ionic phase potential, V
$\phi^{(s)}$	solid phase potential, V
$\boldsymbol{\Phi}_{\alpha\beta}$	dimensionless quantities
Φ	Thiele modulus

Superscripts

(agg)	agglomerate
amb	ambient conditions
(c)	capillary
(C)	carbon
(g)	gas phase
in	inlet
(l)	liquid phase
(m)	membrane
ox	oxidation
(p)	polymer phase
(Pt)	platinum
(PtC)	platinum and carbon
rd	reduction
ref	reference
(s)	solid
sat	saturation

Subscripts

α, β	index for species
a	anode
ave	average
c	cathode
cc	current collector
cell	cell

cl   catalyst layer
eff   effective
fan   fan
ff   flow-fields
gdl   gas diffusion layer
H_2 hydrogen
H_2O water
i species i
j functional layer j
m   membrane
mass   mass
N_2 nitrogen
O_2 oxygen
pot   potential
ref   reference
stack   stack
sp   separator plate
temp   temperature
tot   total
void   void
0   standard conditions

To extend the work on modeling and computational studies of open-cathode PEFC stacks, the aim of the work presented here is threefold: (i) to develop a coupled mathematical model for a PEFC stack, the ambient air, and the fan; (ii) to implement the mathematical model numerically with a one-domain approach, which is commonly used for single cell studies, see for example [24–31]; (iii) to study the interaction between the stack and the fan in terms of placement, fan power and characteristic curves, as well as the size of the cathode flow-field, which can be expected to have a significant impact on the overall pressure drop and hence on the flow rate achieved by the fan.

The layout of the paper is as follows. First, the mathematical model is introduced. It is comprised of two-phase conservation of mass, momentum, species, charge and energy in a fuel cell stack, which is approximated by a repetitive unit cell with periodic boundary conditions. Here, the flow-fields in the anode and cathode are of a porous type (a metallic mesh) and are operating in a co-flow mode. The inherent electrochemistry is accounted for by an agglomerate model and a Butler–Volmer equation in the cathode and the anode catalyst layers, respectively; the membrane is treated with a phenomenological model. For the ambient, conservation of mass, momentum and energy is considered, whilst the fan is approximated with a parameter-adapted polynomial to represent the characteristic curve. Numerically, the mathematical model is then solved via a one-domain approach, that is, the governing equations are solved everywhere; it is therefore necessary to 'suppress' certain equations in domains where they should not be solved. Parameter studies for the system – fuel cell stack, ambient and fan – are then carried out. Finally, conclusions are drawn and extension of the work to include other types of flow-fields and an arbitrary number of fans are highlighted.

2. Mathematical formulation

The mathematical model comprises three components, viz., the fuel cell stack, the ambient, and the fan. The main transport phenomena and assumptions are summarized here, while the full set of equations, boundary and interface conditions, constitutive relations and submodels can be found in Appendices A–E.

2.1. Fuel cell stack

An open-cathode manifold fuel cell stack (see Fig. 1a) is considered with a given number of cells separated from each other by separator plates (sp); each cell, in turn, comprises a membrane (m), two catalyst layers (cl), two gas-diffusion layers (gdl), and two porous flow-fields (ff), as illustrated in Fig. 1b. In this study, the height and width of the stack is kept constant for all cases consid-
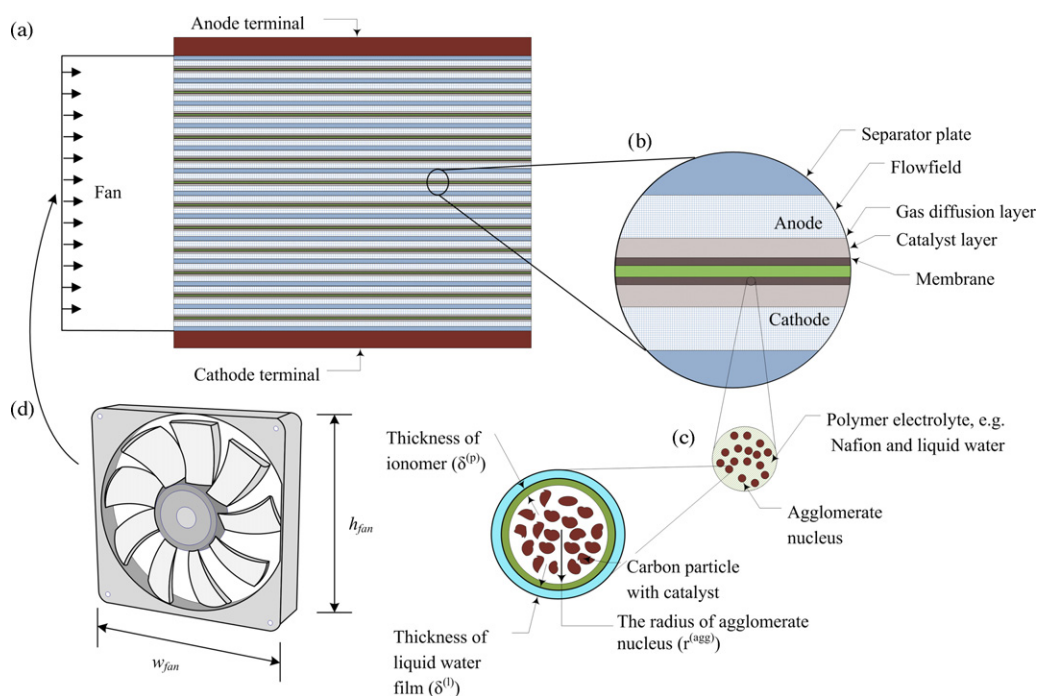
Fig. 1. Schematic of PEFC fuel cell stack with (a) open-cathode manifold and air fan in blowing mode, (b) single cell inside the stack, (c) agglomerate catalyst layer, and (d) fan.
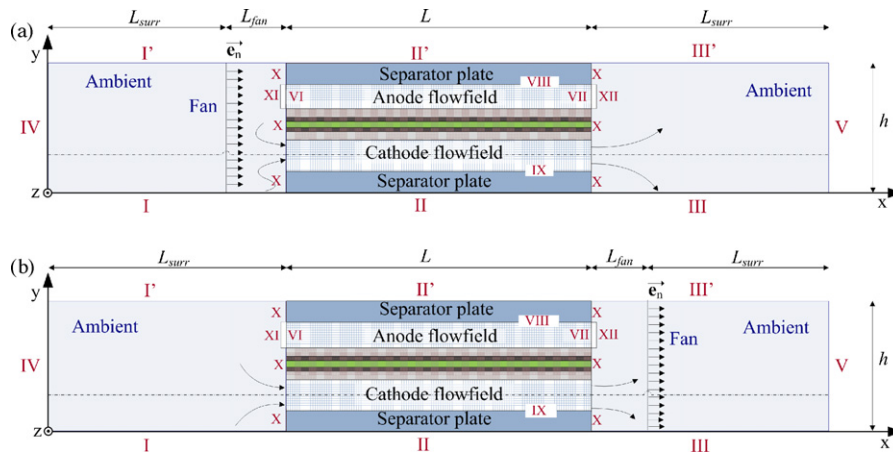
Fig. 2. Repetitive computational domain for the fuel cell model: (a) blowing; (b) suction. Boundaries are marked with roman numerals: periodic ambient conditions (I and I') periodic fuel cell stack unit (II and II'); periodic ambient conditions (III and III'); leftmost ambient (IV); rightmost ambient (V), anode inlet (VI), anode outlet (VII), anode/cathode flow-field and current–collector interface (VIII/IX), wall/insulation (X), surrounding and anode inlet/outlet (XI/XII).

ered and assumed to be the same as those for the fan for simplicity (see Fig. 1d); note that this constraint can easily be relaxed, as more fans or external manifolds can be added to the mathematical framework presented here.

In short, the model accounts for the following transport phenomena:

- *Mass, momentum and species transfer*: Conservation of two-phase mass, momentum and species is considered in the flow-fields, gas-diffusion layers and catalyst layers. The gas phase consists of oxygen, water vapor, hydrogen and nitrogen, whereas the liquid phase is assumed to be only liquid water due to the low solubility of the other gases. Note that all species are solved everywhere (one-domain formulation) but the species that should not be solved in a given half-cell are suppressed; that is to say, no hydrogen and no oxygen in the cathode and anode, respectively. The anode flow-field is not open to the ambient.
- *Energy transfer*: Convection, conduction, evaporation and condensation, ohmic heating, entropy generation and irreversibilities associated with the electrochemical reactions are considered.
- *Charge transfer*: Conservation of charge and Ohm's law are considered.

The main model assumptions/approximations are as follows:

- *Negligible variations in dependent variables in spanwise direction*: The nature of the porous (ff, gdl, cl, and m) and solid layers (sp) allow for a reduction in dimensionality from three to two dimensions (x, y) due to slip conditions and no-mass flux that can be invoked at the walls in the spanwise direction (z), provided the heat flux through these walls is negligible compared with the heat flux in the streamwise direction (x) through each cell in the stack.
- *Repetitive unit cell for the stack*: It is assumed that the stack is sufficiently large that end-effects at the two terminal plates are negligible when solving for the overall stack performance, and that the flow from the fan is uniform so that each individual cell in the stack receives the same flow rate; the model can thus be reduced to a representative unit cell with periodic boundary conditions at the top and lower part of the separator plates (each one is half the height of a separator plate), as illustrated in Fig. 2. The advantage of this approach is that one can consider a stack of an arbitrary number, n_{cell}, of individual cells in series, from which the overall stack power, P_{stack}, and voltage, E_{stack}, can be computed

from

$$P_{stack} = i_{ave}E_{stack}A_{cl}, \tag{1}$$

$$E_{stack} = E_{cell}n_{cell}, \tag{2}$$

where i_{ave} is the average current density of the unit cell and A_{cl} is the area of the catalyst layer in the x and z plane.

- *Thermal equilibrium*: Local thermal equilibrium is assumed between all phases at steady-state.
- *Electrochemistry in catalyst layers*: An agglomerate model (see Appendix E) is implemented to account for mass transfer inside the agglomerates in the cathode catalyst layer (see Fig. 1c). The agglomerate nucleus is taken to be spherical in shape and to be covered by a thin film of ionomer and water. For the anode, a Butler–Volmer equation is sufficient, since the overpotential for the hydrogen oxidation reaction is usually significantly smaller than that for the oxygen reduction reaction.
- *Water transport and properties of membrane*: The membrane model takes into account the flux of water due to electroosmotic drag and diffusion. A GORE membrane is considered, for which the standard phenomenological constitutive relations (water diffusion coefficient and proton conductivity) are modified with a correction factor, similar to [32–34]. Convection of liquid and gas is assumed to be negligible due to the low permeability of the membrane (typically around 10^{-18} m^2[24,35,36]).
- *Two-phase transport*: The standard expressions for the constitutive relations (for example, Leverett function and capillary pressure) are taken as valid for modeling of two-phase transport in the PEFC, see for example [30,34,37–39]. It is further assumed that buoyancy is negligible compared with the flow induced by the capillary pressure throughout the cell (note that flow-fields are porous). Furthermore, a mist flow approximation [29,40,41] is considered and it is assumed that there is no interphase mass transport (evaporation/condensation) in the flow-fields; the latter assumption is found to be necessary in order to ensure a robust numerical code and convergence. The liquid phase is considered to only comprise water due to the low solubility of the other species; but the solubility and transport of the oxygen through a liquid water film in the agglomerates are still taken into account.

2.2. Fan

The performance of a fan is usually given by the relationship between the pressure increase over the fan and the volume flow

rate of the fan, which is known as the characteristic curve of the fan. This curve can typically be expressed as a polynomial function (see Eq. (A.27)) based on fan characteristics measured by the manufacturer; the actual flow velocity is obtained by dividing the volume flow rate with the area normal to the streamwise direction of the fan. The overall velocity that is achieved by the fan for a particular application is thus not known a *priori* but needs to be iterated. If the pressure drop is known in the system at various flow rates, generally referred to as the system characteristic curve, one can find the operating point of the fan by identifying the intersection of the characteristic curves of the fan and the system, as is shown later.

The main assumptions/approximations are:

- *Flow pattern*: The swirl component of the flow induced by the fan is assumed to be negligible [42,43]. Note that this contribution could be added to the overall flow, but that the flow pattern then becomes inherently three-dimensional in nature. Furthermore, the average velocity of the fan is computed such that the flow velocity is uniform through the fan.
- *Laminar flow*: The flow through the fan is assumed to be laminar as a first approximation.
- *Details of fan*: The geometry of the blades, hub, motor and housing of the fan are not resolved; instead we prescribe an interface condition as illustrated in Fig. 2a for blowing and Fig. 2b for suction.

2.3. Ambient

Under ambient conditions, we solve for the following transport phenomena:

- *Mass, momentum and species transfer:* Conservation of two-phase mass, momentum and species (water vapor, nitrogen and oxygen) are accounted for in the surrounding of the fuel cell stack.
- *Energy transfer*: Convection and conduction are solved without any heat generation/dissipation.

The main assumptions/approximations are as follows:

- *Two-phase transport*: It is assumed that there is no interphase mass transfer (evaporation/condensation) in the ambient and that the liquid phase comprises only water.
- *Laminar flow*: The flow in the ambient of the stack is assumed to be laminar as a first approximation.

3. Numerics

The computational domains (see Fig. 2) were created and meshed in the commercial pre-processor software GAMBIT 2.3.16 [44]. After a mesh-independence test, the computational domain was resolved with $\sim 10^5$ elements: a fine *structured* mesh inside the PEFC stack and an increasingly coarser *unstructured* mesh in the ambient in order to reduce the computational cost.

The mathematical model for the stack, fan and ambient comprising 11 dependent variables – $p^{(g)}$, $u^{(g)}$, $v^{(g)}$, $\omega_{H_2}^{(g)}$, $\omega_{O_2}^{(g)}$, $\omega_{H_2O}^{(g)}$, T, $\phi^{(s)}$, $\phi^{(m)}$, s, and λ – was then implemented in the commercial fluid dynamics software FLUENT 6.3 and its fuel cell module, user-defined scalars (UDS) and functions (UDF). In short, the four partial differential equations (PDEs) governing the conservation of $\phi^{(s)}$, $\phi^{(m)}$, s, and λ were implemented with the UDS functionality, and the remaining variables were implemented in the default PDEs of the module; UDFs were used to turn the flow-fields into porous regions, to adjust the default heat generation in the catalyst layers, to mod-

ify the default membrane model settings, and to incorporate the agglomerate model.

In addition, since FLUENT is a *one-domain* finite volume solver, all equations are solved for in the entire computational domain; that is, all PDEs for the stack have to be solved numerically in the ambient as well. It is therefore necessary to fine-tune the parameters and options available in FLUENT to ensure that the dependent variables and their fluxes are close to zero in domains where they are not applicable. Also, the periodic nature of the fuel cell model, the inlet and outlet of the anode, and the fan model require special consideration. In summary, the following strategies were employed to ensure consistency between the mathematical model and the numerical counterpart:

- The dependent variables are set to zero as initial value, low conductivity/diffusivity (magnitude $\sim 10^{-20}$) and no-flux boundaries (at walls between the ambient and stack and at the outer edges of the ambient) to suppress the equations in domains where they are not supposed to be solved.
- A thin numerical layer (10^{-5} m thick) is created at the anode and cathode terminal in order to prescribe Dirichlet boundary conditions for the electronic potential, whilst setting periodic boundary conditions for the temperature (Eqs. (B.1) and (B.2)).
- At the anode inlet and outlet, thin layers (10^{-4} m in thickness) are created to separate the anode inlet and outlet boundaries from the surrounding (see Fig. 2); note that this condition can be relaxed if the stack manifold is implemented for the anode side.
- For the fan model, maximum velocities are set for the polynomial fan curves, u_{fan}^{max}, in order to avoid divergence during iteration (see Table 2).

The numerical model was solved with the Simple algorithm; second-order upwind discretization for the conservation of momentum, species and energy; and first-order upwind discretization for the conservation of charge, liquid water and membrane water content. As an indication of the computational cost, it is noted that on average, around 200–500 iterations are needed for a convergence criteria for all the relative residuals of 10^{-6}; this takes around 15–20 min on a workstation with a quad core processor (1.8 GHz) and 8 GB random access memory (RAM).

4. Results and discussion

Simulations were carried out for typical conditions found in a PEFC with forced air-convection cooling; these base-case conditions together with the geometry and physical parameters are listed in Table 1. The electrochemical parameters were calibrated and validated with experimental polarization curves and local current density distributions obtained with a segmented PEFC equipped with a porous-type flow field [38,45]; see [34] for more details. The representative computational unit cell for the stack is identical in size and properties to the validation case, except that a fan, ambient and periodic boundary conditions are now added. The air flow in the cathode flow-field is provided by a fan in either a blowing or a suction mode; here, a tube-axial fan [46] is employed; all runs are for a blowing mode except for the comparison between blowing and suction discussed later.

Based on the earlier assumption that one representative computational cell can capture the behaviour of the entire stack, which can be expressed as $E_{cell} = E_{stack}/n$, the voltage E_{cell} was varied between 0.9 V and 0.45 V, although the majority of findings refer to a cell operating voltage of 0.7 V, which is a common operating point for the PEFC.

Table 1
Base-case geometry, physical parameters and operating conditions.

Parameter	Value	Units	Reference
A_{cl}	1.071×10^{-2}	m^2	–
A_{fan}	1.4161×10^{-2}	m^2	[46]
$c_{p,H_2}^{(g)}, c_{p,H_2O}^{(g)}, c_{p,O_2}^{(g)}, c_{p,N_2}^{(g)}$	$(14.283, 2.014, 0.919, 1.041) \times 10^3$	$J\,kg^{-1}\,K^{-1}$	–
c_r	100	s^{-1}	[72]
$D_{H_2,0}^{(g)}, D_{H_2O,0}^{(g)}, D_{O_2,0}^{(g)}$	$(11.03, 7.35, 3.23) \times 10^{-5}$	$m^2\,s^{-1}$	[32]
$D_{O_2}^{(l)}$	3.032×10^{-9}	$m^2\,s^{-1}$	[73,68]
$D_{O_2}^{(p)}$	$4.38 \times 10^{-6} \exp(-23848/RT)$	$m^2\,s^{-1}$	[74,64]
E_a	73269	$J\,mol^{-1}$	[74]
$E_{cell}, E_{rev,0}$	0.7, 1.23	V	–, [32]
F	96487	$C\,mol^{-1}$	–
$H_{H_2}^{(p)}$	$2.58 \times 10^3 \exp(170/T)$	$Pa\,m^3\,mol^{-1}$	[75]
$H_{O_2}^{(p)}$	$1.34 \times 10^5 \exp(-666/T)$	$Pa\,m^3\,mol^{-1}$	[69]
$H_{O_2}^{(l)}$	$5.14 \times 10^5 \exp(-498/T)$	$Pa\,m^3\,mol^{-1}$	[69]
H_{vap}	2.26×10^6	$J\,kg^{-1}$	[76]
$h_{cl}, h_{ff,a}, h_{ff,c}, h_{gdl}, h_m, h_{sp}$	$(0.01, 0.5, 1.5, 0.3, 0.05, 0.5) \times 10^{-3}$	m	[38]
j_a^{ref}, j_c^{ref}	$10^9, 275$	$A\,m^{-3}$	[32,34]
$k_{cl}^{(s)}, k_{ff}^{(s)}, k_{gdl}^{(s)}, k_m^{(s)}, k_{sp}^{(s)}$	1.5, 13.3, 1.5, 0.2, 16.3	$W\,m^{-1}\,K^{-1}$	[38,77,38,78,79]
$k_{H_2}^{(g)}, k_{H_2O}^{(g)}, k_{N_2}^{(g)}, k_{O_2}^{(g)}, k^{(l)}$	$(20.28, 2.16, 2.82, 2.89, 67) \times 10^{-2}$	$W\,m^{-1}\,K^{-1}$	[80]
L, L_{surr}, L_{fan}	$(9, 10, 1) \times 10^{-2}$	m	[38], –, –
$M_{H_2}, M_{H_2O}, M_{O_2}, M_{N_2}$	$(2, 18, 32, 28) \times 10^{-3}$	$kg\,mol^{-1}$	–
$M^{(m)}$	1.1	$kg\,mol^{-1}$	[32]
P_{fan}	19.5	W	–
$p^{ref}, p^{amb}, p_0^{(g)}$	101325, 101325, 101325	Pa	[38], –
R	8.314	$J\,mol^{-1}\,K^{-1}$	–
$r^{(agg)}$	10^{-7}	m	[69]
T^{amb}, T_a^{in}, T_0	298.15, 298.15, 298.15	K	–, –, [39]
U_a^{in}	1	$m\,s^{-1}$	–
$\alpha_a^{ox}, \alpha_a^{rd}$	1, 1	–	[32,34]
$\alpha_c^{ox}, \alpha_c^{rd}$	1.5, 1.5	–	[34,34]
$\beta^{(m)}$	0.7	–	[34]
$\varepsilon_{ff}, \varepsilon_{gdl}, \varepsilon_{cl}$	0.9, 0.4, 0.4	–	[38]
θ	0	$^\circ$	[38]
$\kappa_{ff}, \kappa_{gdl}, \kappa_{cl},$	$10^{-8}, 7.3 \times 10^{-13}, 7.3 \times 10^{-13}$	m^2	[81,38,38]
$\mu^{(l)}$	4.7×10^{-4}	$kg\,m^{-1}\,s^{-1}$	[38]
$\mu_{H_2}^{(g)}, \mu_{H_2O}^{(g)}, \mu_{N_2}^{(g)}, \mu_{O_2}^{(g)}$	$(0.841, 1.34, 1.663, 1.919) \times 10^{-5}$	$kg\,m^{-1}\,s^{-1}$	[80]
$\rho^{(C)}, \rho^{(l)}, \rho^{(m)}, \rho^{(Pt)}$	$(1.8, 0.983, 2, 21.45) \times 10^3$	$kg\,m^{-3}$	[69,38,81,69]
$\sigma_{eff,cl}^{(s)}, \sigma_{eff,gdl}^{(s)}$	500, 500	$S\,m^{-1}$	[38,38]
$\sigma_{eff,ff}^{(s)}, \sigma_{eff,sp}^{(s)}$	$(0.1, 1.37) \times 10^6$	$S\,m^{-1}$	[38,79]
τ	6.25×10^{-2}	$N\,m^{-1}$	[39]
$\omega^{(Pt)}$	0.4	–	[81]
c_1, c_2	$-2.1794, 2.953 \times 10^{-2}$	–, K^{-1}	[53]
c_3, c_4	$-9.1837 \times 10^{-5}, 1.4454 \times 10^{-7}$	K^{-2}, K^{-3}	[53]
$\mathfrak{k}_1$	-9×10^{-4}	$V\,K^{-1}$	[32]
$\mathfrak{L}^{(p)}, \mathfrak{L}^{(Pt)}$	$10^{-2}, 0.3 \times 10^{-3}$	$kg\,m^{-2}$	[82,38]
$\mathfrak{H}_a^{in}, \mathfrak{H}^{amb}$	100, 50	%	[38], –
$\mathfrak{T}_0, \mathfrak{T}_1, \mathfrak{T}_2$	273.15, 353.15, 298.15	K	[32]

4.1. Fan and system characteristic behaviour

This study examines five different tube-axial fans with similar design but increasing power rating that are able to drive flow through the stack, viz., 4.5, 12.2, 19.5, 30, and 60 W. The fan characteristic curves, which provide information about the flow rates the fans can sustain for various pressure drops, were taken from the manufacturer [46]. Seventh-order polynomials were then adapted to these curves through curve fitting and found to be sufficiently accurate, as shown in Fig. 3; the coefficients for the polynomials are given in Table 2.

Before implementing the polynomials for the fan in the numerical model, a series of computations ($E_{cell} = 0.7\,V$) was performed by specifying increasing velocities at the fan interface and calculating the respective pressure drops, which provided the system characteristic curve of the stack (see Fig. 3). It is now possible to determine manually the operating point of the fan by locating the intersection between the two characteristic curves; however, the pressure drop over the stack can be expected to be a function of the operating point of the stack, whence it would be necessary to gen-

erate a new system characteristic curve whenever the conditions of the ambient or the stack change (unless the change is negligible). Instead, numerically including the fan through a polynomial as an interface boundary condition (see Appendix A), automatically gives the operating point of the fan as the steady-state solution is iterated.

Returning to Fig. 3, it is noted that the system characteristic curve is located at lower air velocities from the fan, which suggests consideration of a centrifugal fan that can work at higher pressure drops as compared with axial fans. The high pressure drop over the stack originates from the fact that the cathode is equipped with a porous flow-field; changing to, for example, a parallel type of flow-channel should reduce the pressure drop and allow the system characteristic curve to move to the right. Another alternative could be to arrange several axial fans in series, thus increasing the static pressure capability of the fans.

4.2. Fan placement

A further point of interest is the fan placement in a typical PEFC stack with an open-cathode manifold; that is, whether the fan is
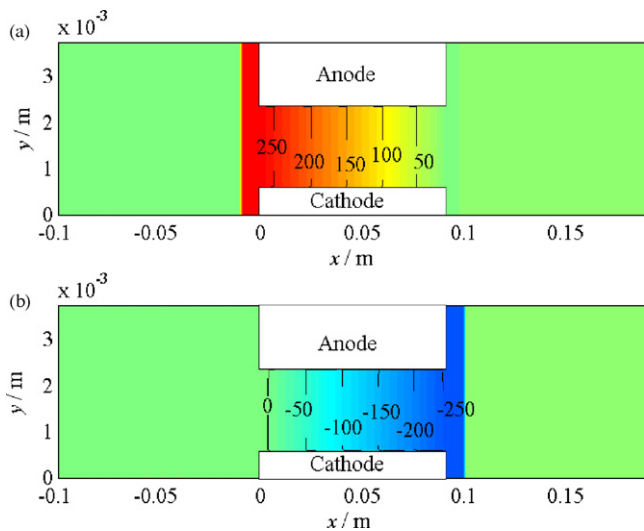
Table 2
Polynomial coefficients and u_{fan}^{max} for fan characteristic curves considered here.

	4.5 W	12.2 W	19.5 W	30 W	60 W
u_{fan}^{max} (m s^{-1})	3.50	4.50	6.00	7.00	8.50
$\mathfrak{C}_1$ (Pa s^7 m^{-7})	−1.20	0	0	−3.00 × 10^{-2}	−1.00 × 10^{-2}
$\mathfrak{C}_2$ (Pa s^6 m^{-6})	15.0	0	−7.00 × 10^{-2}	7.00 × 10^{-1}	38.0
$\mathfrak{C}_3$ (Pa s^5 m^{-5})	−69.0	0.790	1.71	−6.10	−4.20
$\mathfrak{C}_4$ (Pa s^4 m^{-4})	150	−9.21	−14.2	25.0	22.0
$\mathfrak{C}_5$ (Pa s^3 m^{-3})	−160	33.5	53.3	−42.0	−49.0
$\mathfrak{C}_6$ (Pa s^2 m^{-2})	63.0	−34.7	−80.5	27.0	36.0
$\mathfrak{C}_7$ (Pa s m^{-1})	−33.0	−47.6	−10.0	−66.0	−10.0
$\mathfrak{C}_8$ (Pa)	91.0	209	274	360	670
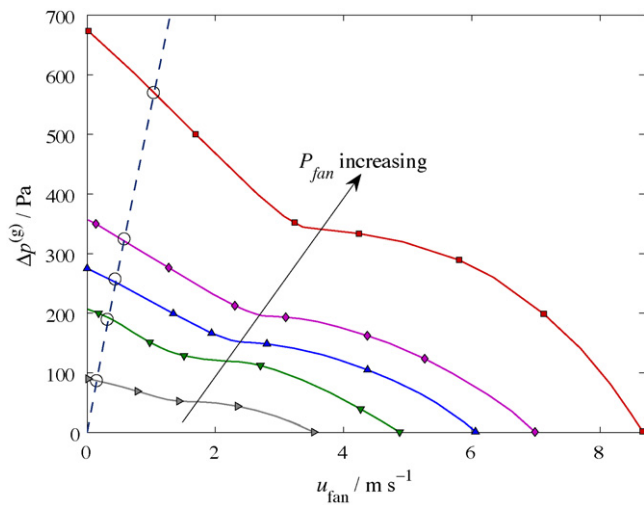
Fig. 3. System characteristic curve for the stack (– –) and fan characteristic curves with symbols denoting data from manufacturer [46] and lines denoting polynomial fits for five different power ratings; viz., 4.5 W (▶), 12.2 W (▼), 19.5 W (▲), 30 W (♦), and 60 W (■). Intersections between stack and fan characteristic curves are given by (○).

placed at the front [47–49] of the stack or at the exit of the stack. The former is generally considered to have one main advantage: the system operates at elevated pressures compared with the ambient, which helps in keeping dust and dirt out of the system [50,51]; however, the air is forced to pass over the hot fan motor, which can heat the air before it enters the system. For the suction-mode, the sys-


Fig. 5. Average current density (–) and corresponding temperature increase (· · ·) for increasing fan power.

tem operates at pressures lower than the ambient and the air passes through the fan as it exits the cathode flow-fields – the air entering the stack is therefore cooler. While the heating arising from the fan motor is not included, it is found that the gauge pressure is above (positive) and below (negative) the ambient for blowing and suction modes, respectively, as illustrated in Fig. 4. On closer inspection, the total pressure drop and all dependent field variables for both modes can be considered identical within the accuracy of the simulation (not shown here), suggesting that the fan placement has no leading order impact on the stack performance. The reason for this behaviour can be found in the large pressure drop over the

Fig. 4. Pressure distribution for base case with fan in either (a) blowing mode or (b) suction mode.
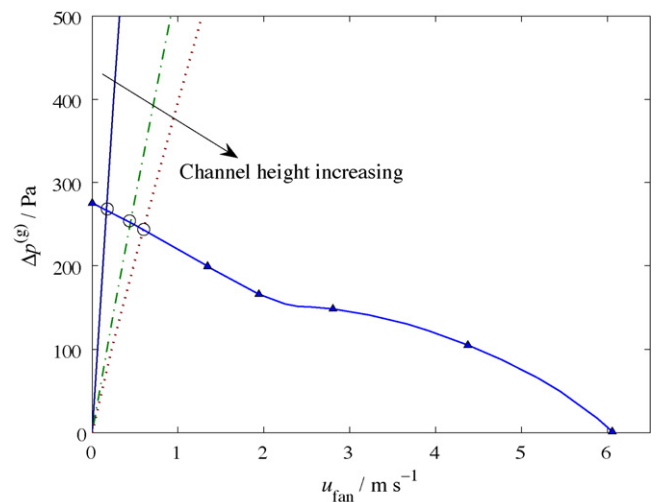
Fig. 6. Characteristic curves for stack with cathode flow-field height of 0.5 mm (–), 1.5 mm (– · –), and 3 mm (· · ·); 19.5 W fan characteristic curve (▲); and intersection between characteristic curves (○).
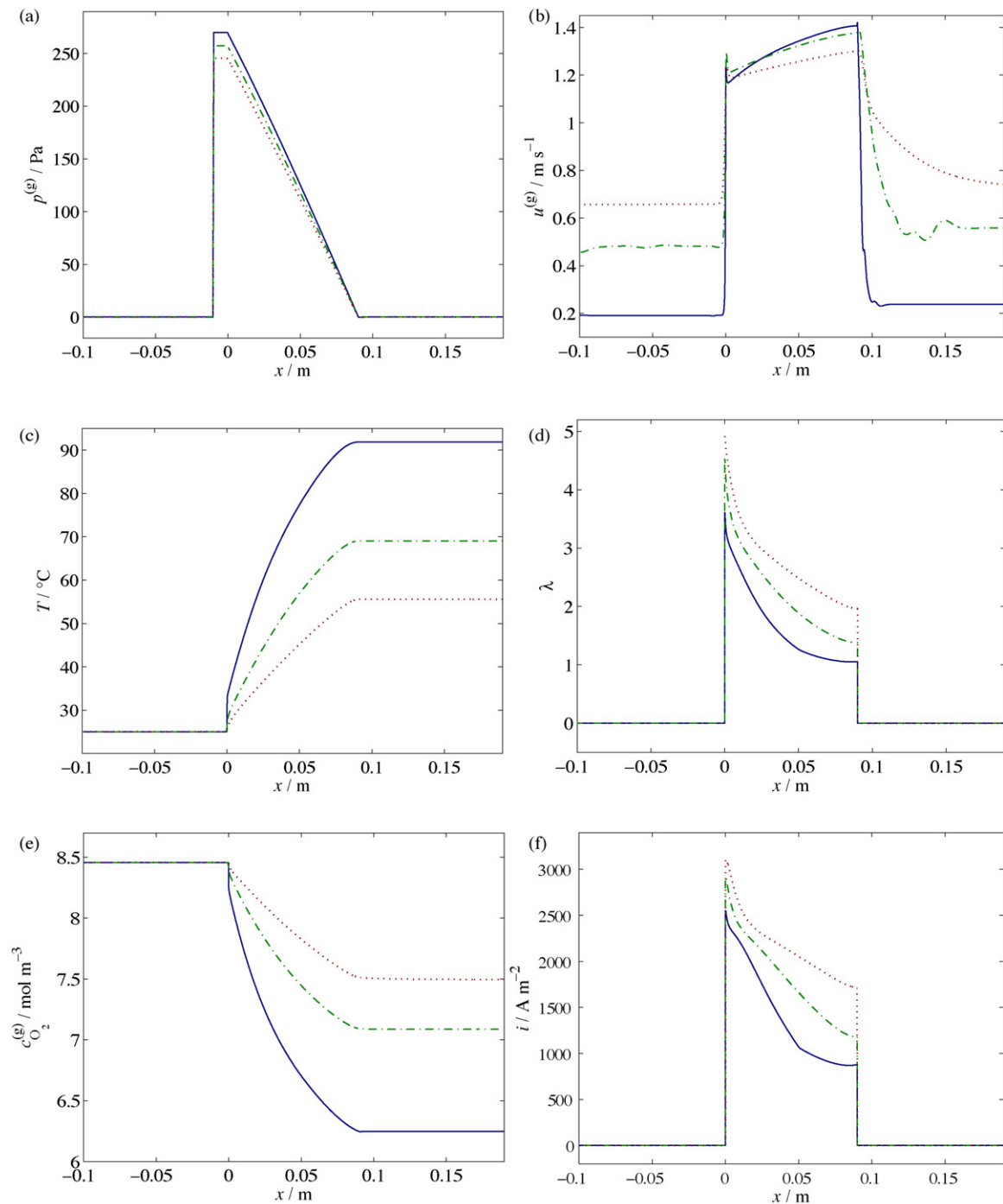
Fig. 7. Local distribution along the middle of the cathode flow-field (ff) or membrane (m) height for the following dependent variables: (a) pressure (ff); (b) streamwise velocity (ff); (c) temperature (ff); (e) oxygen concentration (ff); (d) water content per sulfonic acid group (m); and (f) current density (ff). Three different cathode flow-field heights are considered: 0.5 mm (–), 1.5 mm (– · –), and 3 mm (· · ·).

stack itself, such that the pressure drops associated with the front and end of the stack are negligible.

4.3. Fan power

With respect to the performance of the fuel cell stack, it can be expected that an increase in the power rating of the fan will give rise to higher air flow rates – provided the fan architecture is retained – thus leading to higher air velocities in the cathode flow-field, which translates to a higher oxygen stoichiometry and improved cooling of the stack. This is indeed the case, as can be

inferred from Fig. 5, where an increase in fan power is mirrored by an increase in the average current density of the stack. The current density improves rapidly from around 1400 to 1800 A m^{-2} as the fan power is raised from 4.5 to 20 W, after which the current density increases at a slower rate from around 1800 to 2100 A m^{-2} for fan powers between 20 and 60 W. Conversely, the average fuel cell stack temperature decreases by increasing the fan power from around 70 to 40 °C when the fan power is increased from 4.5 to 60 W; this indicates that a higher air flow rate not only provides higher reactant stoichiometry but also leads to an improved heat transfer rate in this case. The trade-off is, however, the increasing

parasitic load of the fan as its power rating increases, which in turn affects the net power of the stack since it has to power the fan. The model developed here can therefore aid in the selection and fine-tuning of the power rating of the fan(s) to ensure an optimum or near-to-optimum net power output from the stack.

4.4. Cathode flow-field height

In Section 4.1, it was demonstrated that the operating point of the fan is given by the intersection of the characteristic curves for the fan and the system. One can either improve the flow rate of the former by increasing the power of the fan or reduce the pressure drop through the system, which would lead to a shift of the system characteristic curve to the right in Fig. 3. In this particular case, the cathode flow-field is porous in nature, whence an increase in permeability can reduce the pressure drop. Furthermore, a larger flow-field could be expected to decrease the total flow resistance and so lower the pressure drop; however, increasing the flow-field height would lead to a larger stack or less cells overall if the total volume is fixed; the latter, in particular, would lower the overall stack performance, as can be inferred from Eqs. (1) and (2). To study the impact of the height of the cathode flow-field, a fan power of 19.5 W in blowing mode and three different heights of 0.5, 1.5 (base case) and 3 mm are examined. Before investigating the impact on stack performance in detail, the system characteristic curves for the three cathode flow-field heights are determined, as illustrated in Fig. 6. As the height increases the pressure drop decreases, which leads to a shift of the system characteristic curves and intersection with the fan characteristic curve to the right, whence the fan will be able to provide a higher flow rate of air. The local distributions of the key dependent variables through the middle of the cathode flow-field and ambient as well as in the middle of the membrane in the streamwise direction are shown in Fig. 7. Here, several features are apparent; foremost is the jump in gauge pressure from close to zero to the operating pressure of the fan in Fig. 7a, which illustrates how the fan model, given by an interface condition, works. Further, it is clear that an increase in flow-field height gives rise to a lower pressure drop (see Fig. 7a) and overall lower velocity through the cathode (see Fig. 7b) albeit with a higher velocity in the ambient. There is also an increase in the gas velocity in the streamwise direction inside the stack for all heights, which originates from the acceleration of the air in the middle of the flow-field as well as net-flux of water coming out of the cathode gas-diffusion layer into the flow-field. Increasing the height also gives rise to a significant improvement in the cooling rate of the stack (see Fig. 7c), with the temperature dropping from around $94\,^{\circ}$C for the thinnest case (0.5 mm) to around $55\,^{\circ}$C for the thickest (3 mm). The reduction in temperature is mirrored by an increase in the local membrane water content (see Fig. 7d), which in turn provides a higher proton conductivity through the membrane. This, in combination with the increase in oxygen concentration in the streamwise direction (see Fig. 7e), gives rise to an increase in the local current density, as can be inferred from Fig. 7f.

As regards the overall performance of the stack, it is found that an increase in the height of the cathode flow-field reduces the overall stack temperature and improves the overall stack performance at $E_{cell} \lesssim 0.8$ V, as illustrated in Figs. 8 and 9, respectively. The average stack temperature rises from the ambient temperature to $\sim 80\,^{\circ}$C at a current density of $\sim 1500\,\text{A}\,\text{m}^{-2}$ for the thinnest flow-field, which is close to the limiting current density for this case; by contrast, the temperature only rises to $\sim 35\,^{\circ}$C for the thickest channel at this current density. Moreover, the thickest flow-field can sustain a higher current density (up to $3200\,\text{A}\,\text{m}^{-2}$) at a temperature increase of around $\sim 40\,^{\circ}$C. Clearly, the choice of fan and the design of the cathode flow-field when utilizing an open-cathode manifold requires careful consideration to ensure good stack performance.
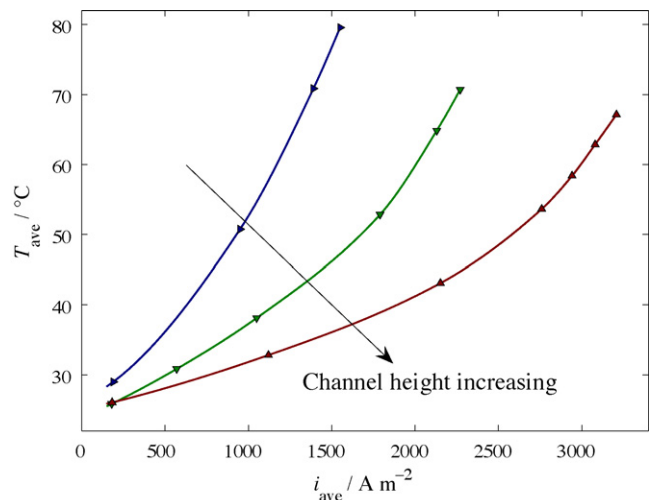
Fig. 8. Comparison of average temperature increase of stack at increasing current densities for three different cathode flow-field heights: 0.5 mm (►), 1.5 mm (▼), and 3 mm (▲).
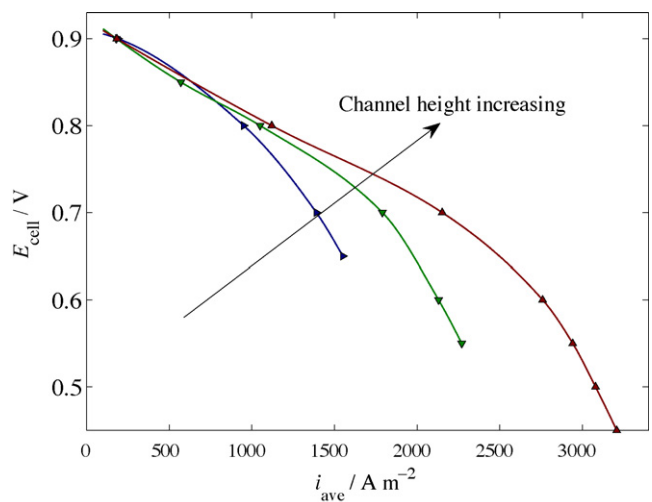
Fig. 9. Comparison of polarization curves for three cathode flow-field heights: 0.5 mm (►), 1.5 mm (▼), and 3 mm (▲).

5. Conclusions

A computational study of forced air-convection in a PEFC stack with an open-cathode manifold has been carried out, where the PEFC stack and ambient are resolved in detail, together with a simple model for the fan based on an interface condition. The computational cost is reduced by identifying a repetitive computational unit cell and by assuming an even flow from the fan, which allows for fast and efficient simulations of the interaction between the fan and the stack. It has also been demonstrated how the fan power and pressure drop over the cathode flow-fields in the stack affect the overall performance as well as the local distribution of the dependent field variables. The fan is of importance in designing an open-cathode manifold PEFC stack as its operation leads to a parasitic load and a reduction in net power from the stack.

The mathematical model derived here and subsequent numerical implementation thus allow for wide-ranging parameter and optimization studies that can aid in the selection of the type of fan (centrifugal or axial), its power rating and placement (for example, distance from the stack), as well as the number of fans that should be employed. The stack performance for fans that are placed in par-

allel or in series can be simulated, depending on the size of the stack and the open cathode manifold.

Other types of flow fields – parallel, serpentine, interdigitated and so forth – can easily be incorporated into the mathematical framework derived here by extending the two-dimensional model to three dimensions.

Acknowledgements

Appendix A. Governing equations

In this paper, the superscripts (g), (l), (s) and (m) denote properties associated with the gas, liquid, solid and membrane, respectively, and (c) denotes any quantity associated with capillary pressure.

A.1. Fuel cell stack

We consider conservation of mass, momentum, energy, species, charge, and two-phase flow expressed as [29,41]:

$$\nabla \cdot \left(\rho^{(g)} \mathbf{u}^{(g)} \right) = S_{\text{mass}} - \dot{m}_{\text{H}_2\text{O}} \quad (\text{ff,gdl,cl}) \tag{A.1}$$

$$\nabla \cdot \left(\rho^{(l)} \mathbf{u}^{(l)} \right) = \dot{m}_{\text{H}_2\text{O}} \quad (\text{ff,gdl,cl}) \tag{A.2}$$

$$\nabla \cdot \left(\rho^{(g)} \mathbf{u}^{(g)} \mathbf{u}^{(g)} \right) = \nabla \cdot \boldsymbol{\sigma} - \frac{\mu^{(g)}}{\kappa} \mathbf{u}^{(g)} \quad (\text{ff,gdl,cl}) \tag{A.3}$$

$$\nabla \cdot \left(\rho^{(g)} c_{\text{p}}^{(g)} \mathbf{u}^{(g)} T \right) = \nabla \cdot (k_{\text{eff}} \nabla T) + S_{\text{temp}} \quad (\text{sp,ff,gdl,cl,m}) \tag{A.4}$$

$$\nabla \cdot \mathbf{n}_i^{(g)} = S_i \quad (\text{ff,gdl,cl}) \tag{A.5}$$

$$\nabla \cdot \mathbf{n}_{\text{H}_2\text{O}}^{(m)} = 0 \quad (\text{m}) \tag{A.6}$$

$$\nabla \cdot \mathbf{i}^{(m)} = S_{\text{pot}} \quad (\text{cl,m}) \tag{A.7}$$

$$\nabla \cdot \mathbf{i}^{(s)} = -S_{\text{pot}} \quad (\text{sp,ff,gdl,cl}) \tag{A.8}$$

In the above equations, $\rho^{(g,l)}$ represent phase densities, $\mathbf{u}^{(g,l)} = (u^{(g,l)}, v^{(g,l)})$ are the phase velocities (in the x and y directions; see Fig. 2), $\dot{m}_{\text{H}_2\text{O}}$ is the interphase mass transfer of water between the gas and the liquid phase, $\boldsymbol{\sigma}$ is the total stress tensor [52], $\mu^{(g,l)}$ are the phase dynamic viscosities, κ is the permeability, $c_{\text{p}}^{(g)}$ is the specific heat capacity, T is the temperature, and k_{eff} is the effective thermal conductivity, and $\mathbf{n}_i^{(g)}$ is the mass flux of species i, while $\mathbf{n}_{\text{H}_2\text{O}}^{(m)}$ is the water flux in the membrane. Furthermore, $\mathbf{i}^{(m)}$ and $\mathbf{i}^{(s)}$ represent the current densities carried by protons and electrons, respectively.

The mass fluxes of species, current densities, liquid water velocity and total stress tensor are defined as

$$\mathbf{n}_i^{(g)} = \rho^{(g)} \mathbf{u}^{(g)} \omega_i^{(g)} - \rho^{(g)} D_{i,\text{eff}}^{(g)} \nabla \omega_i^{(g)} \quad (i = \text{H}_2, \text{O}_2, \text{H}_2\text{O}, \text{N}_2) \tag{A.9}$$

$$\mathbf{n}_{\text{H}_2\text{O}}^{(m)} = \frac{n_{\text{d}} M_{\text{H}_2\text{O}}}{F} \mathbf{i}^{(m)} - \frac{\rho^{(m)}}{M^{(m)}} M_{\text{H}_2\text{O}} D_{\text{H}_2\text{O,eff}}^{(m)} \nabla \lambda \tag{A.10}$$

$$\mathbf{i}^{(m)} = -\sigma_{\text{eff}}^{(m)} \nabla \phi^{(m)} \tag{A.11}$$

$$\mathbf{i}^{(s)} = -\sigma_{\text{eff}}^{(s)} \nabla \phi^{(s)} \tag{A.12}$$

$$\mathbf{u}^{(l)} = \begin{cases} \mathbf{u}^{(g)} s - D^{(c)} \nabla s & (\text{ff}) \\ -D^{(c)} \nabla s & (\text{gdl,cl}) \end{cases} \tag{A.13}$$

$$\boldsymbol{\sigma} = -p^{(g)} \mathbf{I} + \mu^{(g)} [\nabla \mathbf{u}^{(g)} + (\nabla \mathbf{u}^{(g)})^{\text{T}}] - \frac{2}{3} \mu^{(g)} (\nabla \cdot \mathbf{u}^{(g)}) \mathbf{I} \tag{A.14}$$

The model solves for a species mixture of hydrogen (H_2), water (H_2O), oxygen (O_2) and nitrogen (N_2) in the whole domain (note that the hydrogen and oxygen concentrations in the cathode and anode are set to near-zero numerically); $\omega_i^{(g)}$ denotes the mass fraction of species i in the gas phase, and $D_{i,\text{eff}}^{(g)}$ represents the effective diffusivity in the gas phase. The flux of water in the membrane, Eq. (A.10), is expressed with a phenomenological model [53] in terms of the membrane water content, λ, which accounts for the electroosmotic drag (first term on the right hand side [RHS]) and diffusion (second term on the RHS). Here, $D_{\text{H}_2\text{O,eff}}^{(m)}$ is the effective diffusivity of water in the membrane, F is Faraday's constant, $M_{\text{H}_2\text{O}}$ denotes the molecular mass of water, n_{d} is the electroosmotic drag coefficient, $\rho^{(m)}$ and $M^{(m)}$ are the density and equivalent weight of the dry membrane respectively. In Eqs. (A.11) and (A.12), $\phi^{(m)}$ and $\phi^{(s)}$ represent the potentials of the ionic phase and the solid phase respectively, while $\sigma_{\text{eff}}^{(m)}$ and $\sigma_{\text{eff}}^{(s)}$ are the effective electrical conductivities of proton and electron transport respectively. In Eq. (A.13), s is the liquid saturation and $D^{(c)}$ is the capillary diffusion. For the total stress tensor, Eq. (A.14), $p^{(g)}$ is the gas pressure and $\mathbf{I}$ is the identity matrix.

The source terms in Eqs. (A.1)–(A.8) are given by

$$S_{\text{mass}} = \begin{cases} -\dfrac{M_{\text{O}_2} J_c}{4F} + \dfrac{M_{\text{H}_2\text{O}} J_c}{2F} - \nabla \cdot \mathbf{n}_{\text{H}_2\text{O}}^{(m)} & (\text{cathode cl}) \\ -\dfrac{M_{\text{H}_2\text{O}} J_a}{2F} - \nabla \cdot \mathbf{n}_{\text{H}_2\text{O}}^{(m)} & (\text{anode cl}) \\ 0 & (\text{elsewhere}) \end{cases} \tag{A.15}$$

$$S_i = \begin{cases} -\dfrac{M_{\text{O}_2} J_c}{4F} & (\text{O}_2, \text{cathode cl}) \\ +\dfrac{M_{\text{H}_2\text{O}} J_c}{2F} - \nabla \cdot \mathbf{n}_{\text{H}_2\text{O}}^{(m)} - \dot{m}_{\text{H}_2\text{O}} & (\text{H}_2\text{O,cathode cl}) \\ -\nabla \cdot \mathbf{n}_{\text{H}_2\text{O}}^{(m)} - \dot{m}_{\text{H}_2\text{O}} & (\text{H}_2\text{O,anode cl}) \\ -\dot{m}_{\text{H}_2\text{O}} & (\text{H}_2\text{O,gdl}) \\ -\dfrac{M_{\text{H}_2} J_a}{2F} & (\text{H}_2, \text{anode cl}) \\ 0 & (\text{elsewhere}) \end{cases} \tag{A.16}$$

$$S_{\text{pot}} = \begin{cases} -J_c & (\text{cathode cl}) \\ J_a & (\text{anode cl}) \\ 0 & (\text{elsewhere}) \end{cases} \tag{A.17}$$

$$S_{\text{temp}} = \begin{cases} J_c \left(-T \dfrac{\partial E_{\text{rev}}}{\partial T} + |\eta_c| \right) + \sigma_{\text{eff}}^{(m)} (\nabla \phi^{(m)})^2 + \sigma_{\text{eff}}^{(s)} (\nabla \phi^{(s)})^2 + \dot{m}_{\text{H}_2\text{O}} H_{\text{vap}} & (\text{cathode cl}) \\ J_a \eta_a + \sigma_{\text{eff}}^{(m)} (\nabla \phi^{(m)})^2 + \sigma_{\text{eff}}^{(s)} (\nabla \phi^{(s)})^2 + \dot{m}_{\text{H}_2\text{O}} H_{\text{vap}} & (\text{anode cl}) \\ \sigma_{\text{eff}}^{(m)} (\nabla \phi^{(m)})^2 & (\text{m}) \\ \sigma_{\text{eff}}^{(s)} (\nabla \phi^{(s)})^2 + \dot{m}_{\text{H}_2\text{O}} H_{\text{vap}} & (\text{gdl}) \\ \sigma_{\text{eff}}^{(s)} (\nabla \phi^{(s)})^2 & (\text{ff,sp}) \end{cases} \tag{A.18}$$

The source term for mass conservation, S_{mass}, comprises mass consumption and production due to electrochemical reactions and the transport of water through the membrane, whilst the source terms for species conservation, S_i, considers species consumption

and production due to electrochemical reactions as well as inter-phase mass transfer for water and the transport of water through the membrane [41]. In the catalyst layers, λ is found by solving Eqs. (D.1) and (D.2). In the first entry of Eq. (A.18), the first two terms are the reversible and irreversible entropic heat generated by the electrochemical reaction [33], the third and fourth terms describe ohmic heating, whereas the energy transfer due to inter-phase mass transfer is described in the last term, where H_{vap} is the heat of vaporization of water. In Eq. (A.17), $J_{a,c}$ ($J_{a,c} > 0$) denote the volumetric current densities, E_{rev} is the reversible potential, η_a ($\eta_a > 0$) and η_c ($\eta_c < 0$) are the overpotentials at the anode and cathode.

A.2. Ambient

The model solves for conservation of mass, momentum, species, energy and two-phase flow in the surrounding:

$$\nabla \cdot (\rho^{(g)} \mathbf{u}^{(g)}) = 0 \tag{A.19}$$

$$\nabla \cdot (\rho^{(l)} \mathbf{u}^{(l)}) = 0 \tag{A.20}$$

$$\nabla \cdot (\rho^{(g)} \mathbf{u}^{(g)} \mathbf{u}^{(g)}) = \nabla \cdot \boldsymbol{\sigma} \tag{A.21}$$

$$\nabla \cdot \mathbf{n}_i^{(g)} = 0 \tag{A.22}$$

$$\nabla \cdot (\rho^{(g)} c_p^{(g)} \mathbf{u}^{(g)} T) = \nabla \cdot (k_{\text{eff}} \nabla T) \tag{A.23}$$

where the mass flux for species, liquid water velocities and total stress tensor are defined as

$$\mathbf{n}_i^{(g)} = \rho^{(g)} \mathbf{u}^{(g)} \omega_i^{(g)} - \rho^{(g)} D_{i,\text{eff}}^{(g)} \nabla \omega_i^{(g)} \quad (i = H_2O, O_2, N_2) \tag{A.24}$$

$$\mathbf{u}^{(l)} = \mathbf{u}^{(g)} s \tag{A.25}$$

$$\boldsymbol{\sigma} = -p^{(g)} \mathbf{I} + \mu^{(g)} [\nabla \mathbf{u}^{(g)} + (\nabla \mathbf{u}^{(g)})^{\text{T}}] - \frac{2}{3} \mu^{(g)} (\nabla \cdot \mathbf{u}^{(g)}) \mathbf{I} \tag{A.26}$$

A.3. Fan

The fan model is based on the fan characteristic curve, which is introduced as an interfacial condition; the model is represented by a polynomial function that is fitted to data from the manufacturer for the static pressure increase over the fan *vis-á-vis* the flow velocities based on the average conditions at the fan. The overall velocity that is achieved by the fan is thus not known a *priori* but needs to be iterated. The polynomial function is defined as

$$\Delta p_{\text{fan}} = \mathfrak{C}_1 (u_{\text{fan}})^7 + \mathfrak{C}_2 (u_{\text{fan}})^6 + \mathfrak{C}_3 (u_{\text{fan}})^5 + \mathfrak{C}_4 (u_{\text{fan}})^4 + \mathfrak{C}_5 (u_{\text{fan}})^3$$
$$+ \mathfrak{C}_6 (u_{\text{fan}})^2 + \mathfrak{C}_7 u_{\text{fan}} + \mathfrak{C}_8 \tag{A.27}$$

where $\mathfrak{C}_i$ are parameter-adapted constants, Δp_{fan} is the static pressure increase over the fan, and u_{fan} is the velocity through the fan.

Appendix B. Boundary conditions

The boundaries are marked with Roman numerals, as illustrated in Fig. 2.

- At the lower boundaries (I,II,III):

$$\phi^{(s)} = E_{\text{cell}} (\text{II}), \qquad T_{\text{I,II,III}} = T_{\text{I}',\text{II}',\text{III}'} \tag{B.1}$$

- At the upper boundaries (I′, II′, III′):

$$\phi^{(s)} = 0 (\text{II}'), \qquad T_{\text{I}',\text{II}',\text{III}'} = T_{\text{I,II,III}} \tag{B.2}$$

- At the leftmost boundary of the ambient (IV):

$$p^{(g)} = p^{\text{amb}}, \qquad \omega_{O_2}^{(g)} = \omega_{O_2}^{\text{amb}}, \qquad \omega_{H_2O}^{(g)} = \omega_{H_2O}^{\text{amb}},$$
$$T = T^{\text{amb}}, \qquad s = 0 \tag{B.3}$$

- At the rightmost boundary of the ambient (V):

$$p^{(g)} = p^{\text{amb}}, \qquad \frac{\partial \omega_i^{(g)}}{\partial x} = \frac{\partial T}{\partial x} = \frac{\partial s}{\partial x} = 0 \tag{B.4}$$

- At the anode inlet (VI):

$$u^{(g)} = U_a^{\text{in}}, \qquad \omega_{H_2}^{(g)} = \omega_{H_2,a}^{\text{in}}, \qquad \omega_{H_2O}^{(g)} = \omega_{H_2O,a}^{\text{in}}, \qquad \frac{\partial \phi^{(s)}}{\partial x} = 0,$$
$$T = T_a^{\text{in}}, \qquad s = 0 \tag{B.5}$$

- At the anode outlet (VII):

$$p^{(g)} = p^{\text{ref}}, \qquad \frac{\partial \omega_i^{(g)}}{\partial x} = \frac{\partial \phi^{(s)}}{\partial x} = \frac{\partial T}{\partial x} = \frac{\partial s}{\partial x} = 0 \tag{B.6}$$

- At the current collector/flow field interface (VIII and IX):

$$v^{(g)} = 0, \qquad \frac{\partial \omega_i^{(g)}}{\partial y} = \frac{\partial s}{\partial y} = 0 \tag{B.7}$$

- At the stack exterior walls (X):

$$\mathbf{u}^{(g)} = \mathbf{0}, \qquad \frac{\partial \omega_i^{(g)}}{\partial x} = \frac{\partial \phi^{(s)}}{\partial x} = \frac{\partial \phi^{(m)}}{\partial x} = \frac{\partial s}{\partial x} = 0 \tag{B.8}$$

- At the thin layer between the surrounding and the anode inlet (XI):

$$\mathbf{u}^{(g)} = \mathbf{0}, \qquad \frac{\partial \omega_i^{(g)}}{\partial x} = \frac{\partial \phi^{(s)}}{\partial x} = \frac{\partial \phi^{(m)}}{\partial x} = \frac{\partial s}{\partial x} = 0 \tag{B.9}$$

- At the thin layer between the surrounding and the anode outlet (XII):

$$\mathbf{u}^{(g)} = \mathbf{0}, \qquad \frac{\partial \omega_i^{(g)}}{\partial x} = \frac{\partial \phi^{(s)}}{\partial x} = \frac{\partial \phi^{(m)}}{\partial x} = \frac{\partial s}{\partial x} = 0 \tag{B.10}$$

Appendix C. Constitutive relations

The gas density is given by the ideal gas law:

$$\rho^{(g)} = \frac{p^{(g)} M^{(g)}}{RT} \tag{C.1}$$

where R is the gas constant and $M^{(g)}$ denotes the mixture molecular weight given by

$$M^{(g)} = \left(\frac{\omega_{O_2}^{(g)}}{M_{O_2}} + \frac{\omega_{H_2}^{(g)}}{M_{H_2}} + \frac{\omega_{H_2O}^{(g)}}{M_{H_2O}} + \frac{\omega_{N_2}^{(g)}}{M_{N_2}} \right)^{-1} \tag{C.2}$$

The mass fraction of nitrogen is given by

$$\omega_{N_2}^{(g)} = 1 - \omega_{H_2}^{(g)} - \omega_{O_2}^{(g)} - \omega_{H_2O}^{(g)} \tag{C.3}$$

The molar fractions are related to the mass fraction, given by

$$x_i^{(g)} = \frac{\omega_i^{(g)} M^{(g)}}{M_i} \tag{C.4}$$

The molar concentrations are defined as

$$c_i^{(g)} = \frac{\omega_i^{(g)} \rho^{(g)}}{M_i} \tag{C.5}$$

The gas mixture viscosity, $\mu^{(g)}$, is defined as [52]:

$$\mu^{(g)} = \sum_\alpha \frac{x_\alpha^{(g)} \mu_\alpha^{(g)}}{\sum_\beta x_\beta^{(g)} \boldsymbol{\Phi}_{\alpha\beta}} \quad \text{with } \alpha, \beta = H_2, O_2, H_2O, N_2 \tag{C.6}$$

where $x_{\alpha,\beta}^{(g)}$ are the mole fractions of species α and β, and:

$$\Phi_{\alpha\beta} = \frac{\left[1 + (\mu_\alpha/\mu_\beta)^{1/2}(M_\beta/M_\alpha)^{1/4}\right]^2}{\left[8(1 + (M_\alpha/M_\beta))\right]^{1/2}} \tag{C.7}$$

The multicomponent gas mixture thermal conductivity, $k^{(g)}$, is given by

$$k^{(g)} = \sum_\alpha \frac{x_\alpha^{(g)} k_\alpha^{(g)}}{\sum_\beta x_\beta^{(g)} \Phi_{\alpha\beta}} \tag{C.8}$$

The effective thermal conductivity is defined as [54]:

$$k_{\text{eff}} = \varepsilon(1-s)k^{(g)} + \varepsilon s k^{(l)} + (1-\varepsilon)k^{(s)} \tag{C.9}$$

where $k^{(l)}$ is the thermal conductivity of liquid water, ε is the porosity, and $k^{(s)} = (k_{\text{ff}}^{(s)}, k_{\text{gdl}}^{(s)}, k_{\text{cl}}^{(s)}, k_{\text{m}}^{(s)}, k_{\text{sp}}^{(s)})$ are the thermal conductivities of the solid phases in the various functional layers. The gas mixture specific heat capacity, $c_p^{(g)}$, is written as [52]:

$$c_p^{(g)} = \sum_i \omega_i^{(g)} c_{p,i}^{(g)} \tag{C.10}$$

where $c_{p,i}^{(g)} = (c_{p,H_2}^{(g)}, c_{p,O_2}^{(g)}, c_{p,H_2O}^{(g)}, c_{p,N_2}^{(g)})$ are the specific heat capacities of hydrogen, oxygen, water and nitrogen, respectively.

The mass diffusion coefficient for each species i depends on the local temperature and pressure, and is given by

$$D_i^{(g)}(T, p^{(g)}) = \left(\frac{T}{T_0}\right)^{3/2} \left(\frac{p_0^{(g)}}{p^{(g)}}\right) D_{i,0}^{(g)}(T_0, p_0^{(g)}) \tag{C.11}$$

where $D_{i,0}^{(g)}$ is the diffusion coefficient for species i at a given temperature T_0 and gas pressure $p_0^{(g)}$. In the porous media, we apply a Bruggeman correction and consider pore blockage due to the presence of liquid water [55]:

$$D_{i,\text{eff}}^{(g)} = (1-s)\varepsilon^{3/2} D_i^{(g)} \tag{C.12}$$

The relative humidity (%) which determines the water content at the leftmost side of the ambient (IV) and anode inlet (VI) is defined as

$$\mathfrak{H} = \frac{p_{H_2O}^{(g)}}{p_{H_2O}^{\text{sat}}} \times 100 \tag{C.13}$$

where $p_{H_2O}^{(g)}$ is the partial pressure of water vapor, defined as

$$p_{H_2O}^{(g)} = x_{H_2O}^{(g)} p^{(g)} \tag{C.14}$$

and $p_{H_2O}^{\text{sat}}$ is the saturation pressure of water, given as [53]:

$$p_{H_2O}^{\text{sat}} = p^{\text{ref}} \times 10^{c_1 + c_2(T - \mathfrak{T}_0) + c_3(T - \mathfrak{T}_0)^2 + c_4(T - \mathfrak{T}_0)^3} \tag{C.15}$$

The mass fraction of water vapor at the leftmost side of the ambient (IV) can be determined from

$$\omega_{H_2O}^{\text{amb}} = \frac{p_{H_2O}^{\text{sat}} M_{H_2O}(\mathfrak{H}^{\text{amb}}/100)}{p^{(g)} M^{(g)}} \tag{C.16}$$

and the mass fraction of water vapor at the anode inlet (VI) is defined as

$$\omega_{H_2O,a}^{\text{in}} = \frac{p_{H_2O}^{\text{sat}} M_{H_2O}(\mathfrak{H}_a^{\text{in}}/100)}{p^{(g)} M^{(g)}} \tag{C.17}$$

By retaining the ratio $x_{O_2}/x_{N_2} = 21/79$, the mass fraction of oxygen at the ambient can be calculated from

$$\omega_{O_2}^{\text{amb}} = \frac{M_{O_2}}{1 + (79/21)} \left[\frac{1}{M^{(g)}} - \frac{\omega_{H_2O}^{\text{amb}}}{M_{H_2O}}\right] \tag{C.18}$$

while the mass fraction of hydrogen at the anode inlet (VI) is defined as

$$\omega_{H_2,a}^{\text{in}} = 1 - \omega_{H_2O,a}^{\text{in}} \tag{C.19}$$

The average current density is given by

$$i_{\text{ave}} = \frac{1}{L} \int_0^L \mathbf{i}^{(s)} \cdot \mathbf{e}_y \, dx \tag{C.20}$$

where L is the fuel cell length. This integral can be carried out at any cross-section (sp,ff,gdl) of the PEFC stack for which y is constant.

The interphase mass transfer for condensation/evaporation of water is defined as [29,41,56]:

$$\dot{m}_{H_2O} = c_r \max\left((1-s)\frac{p_{H_2O}^{(g)} - p_{H_2O}^{\text{sat}}}{RT} M_{H_2O}, -s\rho^{(l)}\right) \quad \text{(gdl,cl)} \tag{C.21}$$

where c_r is the condensation/evaporation rate constant.

The capillary diffusion for two-phase flow is given by [39,57]:

$$D^{(c)} = -\frac{\kappa s^3}{\mu^{(l)}} \frac{dp^{(c)}}{ds} \tag{C.22}$$

where the capillary pressure, $p^{(c)}$, is given by [57,58]:

$$p^{(c)} = \tau \cos\theta \left(\frac{\varepsilon}{\kappa}\right)^{1/2} \mathcal{J} \tag{C.23}$$

and the Leverett function, $\mathcal{J}$, is defined as

$$\mathcal{J} = 1.417(1-s) - 2.12(1-s)^2 + 1.263(1-s)^3 \tag{C.24}$$

where τ is the surface tension and θ is the wetting angle.

Appendix D. Phenomenological membrane model

The amount of water in the membrane is defined in terms of membrane water content per sulfonic group, λ, which in turn can be expressed as [53]:

$$\lambda = \begin{cases} 0.043 + 17.81a - 39.85a^2 + 36.0a^3 & a \le 1 \\ 14 + 1.4(a-1) & 1 < a \le 3 \end{cases} \tag{D.1}$$

where a is the water activity, given by

$$a = \frac{p_{H_2O}^{(g)}}{p_{H_2O}^{\text{sat}}} + 2s \tag{D.2}$$

Given that a GORE membrane is used, which is a microscopically reinforced composite membrane, a correction factor, $\beta^{(m)}$, is applied for the protonic conductivity, $\sigma^{(m)}$, as well as for the membrane water diffusivity, $D_{H_2O}^{(m)}$ [33]. The effective protonic conductivity is given by [33]:

$$\sigma_{\text{eff}}^{(m)} = \beta^{(m)} \sigma^{(m)} \tag{D.3}$$

where $\sigma^{(m)}$ is defined as [53]:

$$\sigma^{(m)} = (0.5193\lambda - 0.326)\exp\left[1268\left(\frac{1}{303.15} - \frac{1}{T}\right)\right] \tag{D.4}$$

The effective membrane water diffusivity is defined as [33]:

$$D_{H_2O,\text{eff}}^{(m)} = \beta^{(m)} D_{H_2O}^{(m)} \tag{D.5}$$

with $D_{H_2O}^{(m)}$ given by [53,59]:

$$D_{H_2O}^{(m)} = \begin{cases} 3.1 \times 10^{-7} \times \lambda [\exp{(0.28\lambda)} - 1] \exp{\left(-\dfrac{2436}{T}\right)} & \text{for } \lambda \le 3 \\ 4.17 \times 10^{-8} \times \lambda [1 + 161 \exp{(-\lambda)}] \exp{\left(-\dfrac{2436}{T}\right)} & \text{for } \lambda > 3 \end{cases} \quad \text{(D.6)}$$

In addition, the electroosmotic drag is expressed as [53]:

$$n_d = 2.5 \frac{\lambda}{22} \quad \text{(D.7)}$$

In Eq. (D.4), care has to be taken when $\lambda < 0.627$ since the protonic conductivity will be less than zero ($\sigma^{(m)} < 0$); hence, as suggested by Springer et al. [53], we specify that λ cannot become lower than 1. This assumption is justified by Fimrite et al. [60], who showed that the water content in the membrane typically is not lower than 1.5.

Appendix E. Electrochemistry and agglomerate model

The electrochemistry is given by the Butler–Volmer equation at both the anode and cathode side. For the latter, it is further modified by implementing an agglomerate model to account for mass transfer resistances inside the spherical agglomerate [61–66], polymer and liquid water films [41,67–69] which are assumed to cover the agglomerates; that is,

$$J_a = j_a^{ref} \left(\frac{c_{H_2}^{(g)}}{c_{H_2,ref}^{(g)}} \right)^{1/2} \left[\exp{\left(\frac{\alpha_a^{ox} F}{RT} \eta_a \right)} - \exp{\left(\frac{-\alpha_c^{ox} F}{RT} \eta_a \right)} \right] \quad \text{(E.1)}$$

$$J_c = j_c^{ref} \left(\frac{c_{O_2}^{(g)}}{c_{O_2,ref}^{(g)}} \right) \left[-\exp{\left(\frac{\alpha_a^{rd} F}{RT} \eta_c \right)} + \exp{\left(\frac{-\alpha_c^{rd} F}{RT} \eta_c \right)} \right] (1 - \gamma_{cl})$$
$$\times \left(1 - \frac{\gamma^{(p)}}{\gamma^{(agg)}} \right) \frac{RT}{H_{O_2}^{(p)}} \xi_1 \frac{1}{1 + \xi_2 + \xi_3} \quad \text{(E.2)}$$

In Eqs. (E.1) and (E.2), $j_{a,c}^{ref}$ are the volumetric reference exchange current densities; $\alpha_{a,c}^{ox,rd}$ are the transfer coefficients for anode/cathode oxidation/reduction reactions, for simplicity, we assume (as was done previously by [29,36,56]) that $\alpha_a^{ox} = \alpha_a^{rd}$ and $\alpha_c^{ox} = \alpha_c^{rd}$; $c_{H_2,ref}^{(g)}$ and $c_{O_2,ref}^{(g)}$ are the reference concentrations for hydrogen and oxygen respectively; $H_{O_2}^{(p)}$ is the Henry's constant for the air-polymer interface; ξ_1, ξ_2, and ξ_3 are the correction factors due to resistances of the agglomerate, the polymer and liquid water films, respectively. Furthermore, γ_{cl} represents the volume fraction of pores in the catalyst layer, while $\gamma^{(p)}$ and $\gamma^{(agg)}$ are the volume fraction of polymer and agglomerate, respectively.

The cathode volumetric reference exchange current density, j_c^{ref}, is corrected for temperature via an Arrhenius-type relation [61,64]:

$$j_c^{ref} = j_{c,0}^{ref} \exp{\left[-\frac{E_a}{R} \left(\frac{1}{T} - \frac{1}{\mathfrak{T}_1} \right) \right]} \quad \text{(E.3)}$$

It is assumed that the volumetric reference exchange current density of the anode, j_a^{ref}, is constant with a value similar to that used previously [28,32–34,58,70,71]. The reference concentration, $c_{i,ref}^{(g)}$, is given by [69]:

$$c_{i,ref}^{(g)} = \frac{p^{ref}}{H_i^{(p)}} \quad \text{(E.4)}$$

The overpotentials, $\eta_{a,c}$ are defined as

$$\eta_a = \phi^{(s)} - \phi^{(m)} \quad \text{(E.5)}$$
$$\eta_c = \phi^{(s)} - \phi^{(m)} - E_{rev} \quad \text{(E.6)}$$

where the reversible potential, E_{rev}, is written as [38]:

$$E_{rev} = E_{rev,0} + \mathfrak{k}_1 (T - \mathfrak{T}_2) + \frac{RT}{4F} \ln x_{O_2}^{(g)} \quad \text{(E.7)}$$

with $E_{rev,0}$ denoting the reversible potential at standard conditions, and $\mathfrak{k}_1$ and $\mathfrak{T}_2$ are constants given in Table 1. Moreover, the volume fraction of pores in the catalyst layer, volume fraction of polymer and agglomerate given by

$$\gamma_{cl} = \frac{V_{void}}{V_{tot}} = 1 - \gamma^{(agg)} \quad \text{(E.8)}$$

$$\gamma^{(p)} = \frac{V^{(p)}}{V_{tot}} = \frac{\omega^{(p)}}{1 - \omega^{(p)}} \frac{1}{\rho^{(m)}} \frac{\mathfrak{L}^{(Pt)}}{h_{cl} \omega^{(Pt)}} \quad \text{(E.9)}$$

$$\gamma^{(agg)} = \frac{V^{(agg)}}{V_{tot}} = \gamma^{(p)} + \gamma^{(PtC)} \quad \text{(E.10)}$$

with

$$V^{(agg)} = V^{(PtC)} + V^{(p)}, \qquad V_{void} = V^{(g)} + V^{(l)},$$
$$V_{tot} = V^{(agg)} + V_{void} = V^{(PtC)} + V^{(p)} + V^{(g)} + V^{(l)},$$

where in Eq. (E.9), $\mathfrak{L}^{(Pt)}$ is the platinum loading, $\omega^{(Pt)}$ is the mass fraction of platinum loading on carbon, V_{tot} is the total volume in catalyst layer and $\omega^{(p)}$ is the mass fraction of polymer loading in the catalyst layer, defined as

$$\omega^{(p)} = \frac{\mathfrak{L}^{(p)}}{\mathfrak{L}^{(Pt)} + \mathfrak{L}^{(C)} + \mathfrak{L}^{(p)}} \quad \text{(E.11)}$$

where $\mathfrak{L}^{(p)}$ is the polymer loading and $\mathfrak{L}^{(C)}$ is the carbon loading, expressed as

$$\mathfrak{L}^{(C)} = \frac{\mathfrak{L}^{(Pt)}}{\omega^{(Pt)}} - \mathfrak{L}^{(Pt)} \quad \text{(E.12)}$$

The volume fraction of platinum and carbon, $\gamma^{(PtC)}$, in Eq. (E.10) is defined as

$$\gamma^{(PtC)} = \frac{V^{(PtC)}}{V_{tot}} = \left[\frac{1}{\rho^{(Pt)}} + \frac{1 - \omega^{(Pt)}}{\rho^{(C)} \omega^{(Pt)}} \right] \frac{\mathfrak{L}^{(Pt)}}{h_{cl}} \quad \text{(E.13)}$$

with $\rho^{(Pt)}$ denoting the platinum density.

The correction factor, ξ_1, is defined as [62,64,69]:

$$\xi_1 = \frac{1}{\Phi} \left[\frac{1}{\tanh{(3\Phi)}} - \frac{1}{3\Phi} \right] \quad \text{(E.14)}$$

where Φ is the Thiele modulus, given by

$$\Phi = \frac{r^{(agg)}}{3} \sqrt{\frac{k_c}{D_{O_2,eff}^{(agg)}}} \quad \text{(E.15)}$$

Here, $r^{(agg)}$ is the agglomerate radius, and k_c is the reaction rate constant, defined as [61–66]:

$$k_c = \frac{j_c^{ref} (1 - (\gamma^{(p)}/\gamma^{(agg)})) (-\exp{((\alpha_a^{rd} F/RT)\eta_c)} + \exp{((-\alpha_c^{rd} F/RT)\eta_c)})}{4F c_{O_2,ref}^{(g)}} \quad \text{(E.16)}$$

The effective diffusion coefficient of oxygen in the polymer inside agglomerate, $D_{O_2,eff}^{(agg)}$, is given by the diffusion coefficient of oxygen in the polymer film, $D_{O_2}^{(p)}$, with Bruggeman correlation [61,65] as

$$D_{O_2,eff}^{(agg)} = D_{O_2}^{(p)} \left(\frac{\gamma^{(p)}}{\gamma^{(agg)}} \right)^{1.5} \quad \text{(E.17)}$$

The correction factor due to the polymer film, ξ_2, is calculated as [69]:

$$\xi_2 = \frac{\delta^{(p)}}{D_{O_2}^{(p)}} \frac{\xi_1}{a^{(p)}} k_c \quad \text{(E.18)}$$

where the polymer thickness, $\delta^{(p)}$, is defined as

$$\delta^{(p)} = \sqrt[3]{(r^{(agg)})^3 \left(1 + \frac{\gamma^{(p)}}{\gamma^{(PtC)}}\right)} - r^{(agg)} \qquad (E.19)$$

In Eq. (E.18), the agglomerate surface area per unit volume of catalyst layer, $a^{(p)}$, is given by

$$a^{(p)} = 4\pi n^{(agg)}(r^{(agg)} + \delta^{(p)})^2 \qquad (E.20)$$

where $n^{(agg)}$ is the number of agglomerates per unit volume, defined as

$$n^{(agg)} = \frac{3\gamma^{(agg)}}{4\pi(r^{(agg)} + \delta^{(p)})^3} \qquad (E.21)$$

Finally, the correction factor representing mass transfer resistance due to liquid water film, ξ_3, is expressed as [69]:

$$\xi_3 = \frac{\delta^{(l)}}{D_{O_2}^{(l)}} \frac{\xi_1}{a^{(l)}} k_c \frac{H_{O_2}^{(l)}}{H_{O_2}^{(p)}} \qquad (E.22)$$

where $H_{O_2}^{(l)}$ is Henry's constant for the air-water interface, $D_{O_2}^{(l)}$ is the diffusion coefficient of oxygen in the liquid water, $\delta^{(l)}$ is the thickness of liquid water film and $a^{(l)}$ is the surface area of the agglomerate including liquid water per unit volume defined as

$$\delta^{(l)} = \sqrt[3]{(r^{(agg)} + \delta^{(p)})^3 \left(1 + \frac{\gamma^{(l)}}{\gamma^{(agg)}}\right)} - (r^{(agg)} + \delta^{(p)}) \qquad (E.23)$$

$$a^{(l)} = 4\pi n^{(agg)}(r^{(agg)} + \delta^{(p)} + \delta^{(l)})^2 \qquad (E.24)$$

where the volume fraction of liquid water, $\gamma^{(l)}$, is expressed as function of the liquid saturation, s, by

$$\gamma^{(l)} = \frac{V^{(l)}}{V_{tot}} = s\gamma_{cl} \qquad (E.25)$$

References

[1] J. Larminie, A. Dicks, Fuel Cell Systems Explained, second ed., Wiley, 2003.
[2] K.S. Dhathathreyan, N. Rajalakshmi, in: S. Basu (Ed.), Recent Trends in Fuel Cell Science and Technology, Anamaya Publisher, 2007.
[3] X. Zang, T. Wang, J.Z.D. Zhen, Y. Zhang, L. Zhu, C. Chen, J. Yan, H. Liu, Y. Lou, X. Li, B. Xia, Int. J. Electrochem. Sci 2 (2007) 618–626.
[4] F. Laurencelle, R. Chahire, J. Hamelin, K. Agbassou, T. Bose, A. Laperriere, Fuel Cells 1 (2001) 66–71.
[5] Z. Qi, A. Kaufman, J. Power Sources 109 (2002) 469–476.
[6] P. Rodatz, F. Buchi, C. Onder, L. Guzzela, J. Power Sources 128 (2004) 208–217.
[7] R. Eckl, W. Zehtner, C. Liu, U. Wagner, J. Power Sources 138 (2004) 137–144.
[8] Y. Sohn, G. Park, T. Yang, Y. Yoon, C.K.W.Y. Lee, S.D. Yim, J. Power Sources 145 (2005) 604–609.
[9] L. Dumercy, M. Pera, R. Glises, D. Hisel, S. Hamandi, F. Badin, J. Kauffman, Fuel Cells 4 (2004) 352–357.
[10] Y. Yim, Y. Sohn, Y. Yoon, S. Um, C. Kim, W. Lee, J. Power Sources 178 (2008) 711–715.
[11] T. Tanaka, K. Otsuka, K. Oyakawa, S. Watanabe, J. Power Sources 147 (2005) 208–213.
[12] Z. Liu, Z. Mao, C. Wang, W. Zhuge, Y. Zhang, J. Power Sources 160 (2006) 1111–1121.
[13] Y. Shan, S. Choe, J. Power Sources 158 (2006) 274–286.
[14] Y. Shan, S. Choe, S. Choi, J. Power Sources 165 (2007) 196–209.
[15] S. Shimpalee, M. Ohashi, J.V. Zee, C. Ziegler, C. Stoeckmann, C. Sadeler, C. Hebling, Electrochim. Acta 54 (2009) 2899–2911.
[16] A.A. Kulikovsky, SIAM J. Appl. Math. 70 (2009) 531–542.
[17] S. Lister, J.G. Pharoah, G. McLean, N. Djilali, J. Power Sources 156 (2005) 334–344.
[18] Y. Zhang, R. Pitchumani, Int. J. Heat Mass Transfer 50 (2007) 4698–4712.
[19] B.P.M. Rajani, A.K. Kolar, J. Power Sources 164 (2007) 210–221.
[20] Y. Wang, T.H. Yang, W.Y. Lee, J. Ke, C.S. Kim, J. Power Sources 145 (2005) 572–581.
[21] Y. Wang, Y.J. Sohn, W.Y. Lee, J. Ke, C.S. Kim, J. Power Sources 145 (2005) 563–571.
[22] Y. Wang, J. Ke, W.Y. Lee, T.H. Yang, C.S. Kim, Int. J. Hydrogen Energy 30 (2005) 1351–1361.
[23] Y. Wang, M. Ouyang, J. Power Sources 164 (2007) 721–729.
[24] V. Gurau, H. Liu, S. Kakac, AIChE J. 44 (1998) 2410–2422.
[25] T. Zhou, H. Liu, Int. J. Transport Phenomena 3 (2001) 177–198.
[26] S. Um, C.Y. Wang, K.S. Chen, J. Electrochem. Soc. 147 (2000) 4485–4493.
[27] N.P. Siegel, M.W. Ellis, D.J. Nelson, M.R. von Spakovsky, J. Power Sources 115 (2003) 81–89.
[28] S. Um, C.Y. Wang, J. Power Sources 125 (2004) 40–51.
[29] S. Li, U. Becker, ASME Fuel Cell Science, Proceeding of the Second Engineering and Technology Conference, Rochester, NY, 2004.
[30] N.P. Siegel, M.W. Ellis, D.J. Nelson, M.R. von Spakovsky, J. Power Sources 128 (2004) 173–184.
[31] D. Cheddie, N. Munrofor, J. Power Sources 147 (2005) 72–84.
[32] H. Ju, C.-Y. Wang, S. Cleghorn, U. Beuscher, J. Electrochem. Soc. 152 (2005) A1645–A1653.
[33] H. Ju, H. Meng, C.-Y. Wang, Int. J. Heat Mass Transfer 48 (2005) 1303–1315.
[34] A.P. Sasmito, E. Birgersson, A.S. Mujumdar, Heat Transfer Eng. 32 (2011), doi:10.1080/01457631003769302, in press.
[35] D.M. Bernardi, M.W. Verbrugge, J. Electrochem. Soc. 139 (1992) 2477–2490.
[36] T. Berning, D.M. Lu, N. Djilali, J. Power Sources 106 (2002) 284–294.
[37] J.H. Nam, M. Kaviany, Int. J. Heat and Mass Transfer 46 (2003) 4595–4611.
[38] M. Noponen, E. Birgersson, J. Ihonen, M. Vynnycky, A. Lundblad, G. Lindbergh, Fuel Cells 4 (2004) 365–377.
[39] E. Birgersson, M. Noponen, M. Vynnycky, J. Electrochem. Soc. 152 (2005) A1021–A1034.
[40] H. Meng, C.-Y. Wang, J. Electrochem. Soc. 152 (2005) A1733–A1741.
[41] D.H. Schwarz, N. Djilali, J. Electrochem. Soc. 154 (2007) B1167–B1178.
[42] A. Nakayama, N. Kokubo, T. Ishida, F. Kuwahara, Numer. Heat Transfer, Part A 37 (2000) 155–165.
[43] P.G. Tucker, J. Fluids Eng 123 (2001) 372–381.
[44] Fluent 6.3.26, http://www.fluent.com, cited 2008.
[45] M. Noponen, J. Ihonen, A. Lundblad, G. Lindbergh, J. Appl. Electrochem. 34 (2004) 255–262.
[46] ebmpapst fan, http://www.ebmpapst.us, 2009.
[47] D.S. Rosa, D. Pinto, V. Silva, R. Silva, C.M. Rangel, Int. J. Hydrogen Energy 32 (2007) 4350–4357.
[48] G. Jung, K. Lo, A. Su, F. Weng, C. Tu, T. Yang, S. Chan, Int. J. Hydrogen Energy 33 (2008) 2980–2985.
[49] J. Wu, S. Galli, I. Lagana, A. Pozio, G. Monetelone, X. Yuan, J. Power Sources 188 (2009) 199–204.
[50] W.T.W.B. Cory, Fans and Ventilation: A Practical Guide, Elsevier, 2005.
[51] D.S. Steinberg, Cooling Technique for Electronic Equipment, 2nd ed., John Wiley and Sons, 1991.
[52] R.B. Bird, W.E. Stewart, E.N. Lightfoot, Transport Phenomena, 2nd ed., Wiley, 2002.
[53] T. Springer, T.A. Zawodzinski, S. Gottesfeld, J. Electrochem. Soc. 138 (1991) 2334–2342.
[54] J.J. Baschuk, X. Li, J. Power Sources 142 (2004) 134–153.
[55] D.A.G. Bruggeman, Ann. Phys. (Leipzig) 24 (1935) 636–679.
[56] A.D. Le, B. Zhou, J. Power Sources 193 (2009) 665–683.
[57] M. Kaviany, Principles of Heat Transfer in Porous Media, 1st ed., Springer-Verlag, 1995.
[58] Z.H. Wang, C.-Y. Wang, K.S. Chen, J. Power Sources 94 (2001) 40–50.
[59] S. Motupally, A.J. Becker, J.W. Weidner, J. Electrochem. Soc. 147 (2000) 3171–3177.
[60] J. Fimrite, H. Struchtrup, N. Djilali, J. Electrochem. Soc. 152 (2005) A1804–A1814.
[61] W. Sun, B.A. Peppley, K. Karan, Electrochim. Acta 50 (2005) 3359–3374.
[62] M. Secanell, K. Karan, A. Suleman, N. Djilali, Electrochim. Acta 52 (2007) 6318–6337.
[63] J.G. Pharoah, K. Karan, W. Sun, J. Power Sources 161 (2006) 214–224.
[64] D. Harvey, J.G. Pharoah, K. Karan, J. Power Sources 179 (2008) 209–219.
[65] F. Jaouen, G. Lindbergh, G. Sundholm, J. Electrochem. Soc. 149 (2002) A437–A447.
[66] E. Birgersson, M. Vynnycky, J. Power Sources 153 (2006) 76–88.
[67] G. Lin, W. He, T.V. Nguyen, J. Electrochem. Soc. 151 (2004) A1999–A2006.
[68] W.W. Yang, T.S. Zhao, Electrochim. Acta 52 (2007) 6125–6140.
[69] R.M. Rao, D. Bhattacharya, R. Rengaswamy, S.R. Choudhury, J. Power Sources 173 (2007) 375–393.
[70] Y. Wang, C.-Y. Wang, Electrochim. Acta 50 (2005) 1307–1315.
[71] H. Ju, C.-Y. Wang, J. Electrochem. Soc. 151 (2004) A1954–A1960.
[72] D. Natarajan, T.V. Nguyen, J. Electrochem. Soc. 148 (2001) A1324–A1335.
[73] D. Song, Q. Wang, Z.-S. Liu, T. Navessin, M. Eikerling, S. Holdcroft, J. Power Sources 126 (2004) 104–111.
[74] A. Parthasarathy, S. Srinivasan, J.A. Appleby, C.R.G. Martin, J. Electrochem. Soc. 139 (1992) 2334–2342.
[75] R.F. Mann, J.C.A.B.A. Peppley, C.P. Thurgood, J. Power Sources 161 (2006) 768–774.
[76] Y. Wang, C.-Y. Wang, J. Electrochem. Soc. 153 (2006) A1193–A1200.
[77] E. Karawacki, B.M. Suleiman, Meas. Sci. Technol. 2 (1991) 744–750.
[78] P.J.S. Vie, S. Kjelstrup, Electrochim. Acta 49 (2004) 1069–1077.
[79] B.R. Padhy, R.G. Reddy, J. Power Sources 153 (2006) 125–129.
[80] D.R. Lide, CRC Handbook of Chemistry and Physics, 89th ed., CRC Press/Taylor and Francis, Boca Raton, FL, 2009.
[81] H. Ly, E. Birgersson, M. Vynnycky, A.P. Sasmito, J. Electrochem. Soc. 156 (2009) B1156–B1168.
[82] M. Han, J.H. Xu, S.H. Chan, S.P. Jiang, Electrochim. Acta 53 (2008) 5361–5367.